



**HAL**  
open science

## **TAK1-binding protein 1 is a pseudophosphatase**

Sarah H Conner, Gursant Kular, Mark Peggie, Sharon Shepherd, Alexander W Schüttelkopf, Philip Cohen, Daan M F van Aalten

► **To cite this version:**

Sarah H Conner, Gursant Kular, Mark Peggie, Sharon Shepherd, Alexander W Schüttelkopf, et al.. TAK1-binding protein 1 is a pseudophosphatase. *Biochemical Journal*, 2006, 399 (3), pp.427-434. 10.1042/BJ20061077 . hal-00478633

**HAL Id: hal-00478633**

**<https://hal.science/hal-00478633>**

Submitted on 30 Apr 2010

**HAL** is a multi-disciplinary open access archive for the deposit and dissemination of scientific research documents, whether they are published or not. The documents may come from teaching and research institutions in France or abroad, or from public or private research centers.

L'archive ouverte pluridisciplinaire **HAL**, est destinée au dépôt et à la diffusion de documents scientifiques de niveau recherche, publiés ou non, émanant des établissements d'enseignement et de recherche français ou étrangers, des laboratoires publics ou privés.

# TAK1-binding protein 1 is a pseudo-phosphatase

Sarah H. Conner<sup>1,+</sup>, Gursant Kular<sup>1,+</sup>, Mark Peggie<sup>1,+</sup>, Sharon Shepherd<sup>2,+</sup>,

Alexander W. Schüttelkopf<sup>2</sup>, Philip Cohen<sup>1</sup>, and Daan M. F. van Aalten<sup>2,\*</sup>

<sup>1</sup> MRC Protein Phosphorylation Unit, and

<sup>2</sup> Division of Biological Chemistry & Molecular Microbiology,

School of Life Sciences, University of Dundee, Dundee DD1 5EH, Scotland.

+ These authors contributed equally to the work.

\* To whom correspondence should be addressed.

E-mail: [dava@davapc1.bioch.dundee.ac.uk](mailto:dava@davapc1.bioch.dundee.ac.uk), Fax: ++ 44 1382 345764

Running title: Structure of TAB1

Keywords: protein phosphatase, TAB1, TAK1, inflammation, proinflammatory cytokine, X-ray crystallography

## Abstract

TAB1 (TAK1-binding protein 1) is one of the regulatory subunits of TGF $\beta$ -activated kinase 1 (TAK1), a protein kinase that lies at the head of three pro-inflammatory kinase cascades. Here we report the crystal structure of the N-terminal domain of TAB1. Surprisingly, TAB1 possesses a fold closely related to that of the PPM phosphatase family as demonstrated by the close structural similarity with protein phosphatase 2C $\alpha$ . However, we were unable to detect any phosphatase activity for TAB1 using a phosphopeptide or *p*-nitrophenyl phosphate as substrates. Although the overall protein phosphatase 2C $\alpha$  fold is conserved in TAB1, detailed structural analyses and mutagenesis studies show that several key residues required for dual metal binding and catalysis are not present in TAB1, although binding of a single metal is supported by soaking experiments with manganese and isothermal titration calorimetry. Thus, it appears that TAB1 is a “pseudophosphatase”, possibly binding to and regulating accessibility of phosphorylated residues on substrates downstream of TAK1 or on the TAK1 complex itself.

## Abbreviations

ERK1/2, extracellular signal-regulated kinase 1/2; IL-1, interleukin-1; ITC, isothermal titration microcalorimetry; JNK1/2, c-Jun N-terminal protein kinase 1/2; LPS, lipopolysaccharide; MAPK, mitogen activated protein kinase; MRC, Medical Research Council; NF $\kappa$ B, nuclear factor  $\kappa$ B; PP2C, protein phosphatase 2C; PPM, Mg<sup>2+</sup>- or Mn<sup>2+</sup>-dependent protein phosphatase; PTP, protein tyrosine phosphatase; RMSD, root mean square deviation; STYX, phosphoserine, phosphothreonine or phosphotyrosine interaction protein; TAB1/2/3, TAK1-binding protein 1/2/3; TAK1, TGF $\beta$ -activated kinase 1; TNF, tumour necrosis factor.

## Introduction

TGF $\beta$ -activated protein kinase 1 (TAK1) is activated when cells are stimulated with bacterial lipopolysaccharide (LPS) or the pro-inflammatory cytokines tumour necrosis factor (TNF) and interleukin-1 (IL-1). It plays a key role in switching on several pro-inflammatory signalling pathways, including those that activate the mitogen activated protein kinases (MAPKs), termed p38 $\alpha$  MAPK, JNK1/2 and ERK1/2, as well as the transcription factor NF $\kappa$ B (Fig. 1A) [1, 2].

TAK1 is complexed to two other proteins in cells, namely TAK1-binding protein 1 (TAB1) and either TAB2 or the structurally related TAB3 [3]. The activation of TAK1 by LPS or IL-1 is thought to be triggered by the formation of Lys63-linked polyubiquitylated TNF receptor associated factor 6 (TRAF6) and its interaction with the ring finger domains of TAB2/TAB3 [4]. This induces phosphorylation of the activation loop of TAK1, resulting in its activation.

We have shown that the extent of activation of TAK1 in cells is limited by a feedback control mechanism in which p38 $\alpha$  MAPK down-regulates TAK1 [5, 3] (Fig. 1A). This is mediated by the p38 $\alpha$  MAPK-catalysed phosphorylation of TAB1 at Ser423 and Thr431 [5] and/or by the phosphorylation of TAB2/TAB3 at sites that have yet to be defined [3]. The feedback loop provides a mechanism for coordinating the degree of activation of several pro-inflammatory signalling pathways and has important implications for the development of anti-inflammatory drugs. Thus, inhibitors of p38 $\alpha$  MAPK show efficacy in animal models of rheumatoid arthritis [6] and a number of these compounds have entered human clinical trials. However, these inhibitors also cancel the feedback control of TAK1, causing the hyperactivation of JNK and a more rapid activation of NF $\kappa$ B [5]. This may underlie some of the side effects of these drugs, which have prevented them, thus far, from advancing to later stage clinical trials.

It has been noticed that the N-terminal region of TAB1 shares weak homology with protein phosphatase 2C [7], a member of the PPM family of protein serine/threonine phosphatases. In contrast, the C-terminal region contains a docking site for p38 $\alpha$  MAPK (between residues 371 and 436) [5, 8] and the TAK1-binding domain (which lies within the C-terminal 68 residues of TAB1) [9, 10, 11]. The three-dimensional structure of a chimaeric protein in which the TAK1 catalytic subunit is fused covalently to the C-terminal 36 residues of TAB1 has recently been reported [12] and interaction with this  $\alpha$ -helical fragment of TAB1 is sufficient to activate the TAK1 catalytic subunit. In this paper, we describe the three-dimensional structure of the N-terminal domain of TAB1 determined by X-ray crystallography. Strikingly, the structure of TAB1 resembles that of PP2C with the addition of an unusual “stalk”-like domain. However, dramatic changes in the active site residues are observed. These changes, which we probed by mutagenesis and phosphatase assays, imply that TAB1 is no longer able to bind the two metal ions required for catalysis by PP2C, suggesting that it is unlikely to possess any phosphatase activity. Potential functions for this unusual “pseudophosphatase” are discussed in the light of these results.

## Results

### Structure of the TAB1 N-terminal domain

Full length TAB1 was overexpressed in *E. coli*, but failed to crystallise. Using limited proteolysis in combination with mass determination and N-terminal sequencing, a trypsin resistant fragment was identified (residues 7-402), which readily overexpressed in *E. coli* as a GST-fusion protein (25 mg/l bacterial culture). Affinity purification followed by cleavage with PreScission protease and further ion exchange chromatography in the absence of divalent cations yielded pure protein (15 mg from 1 l of bacterial culture), which was concentrated to 10 mg/ml and crystallised from lithium sulphate solutions. The crystals obtained were very fragile. Rotating anode and synchrotron diffraction data were collected on the native crystals (Table I). Soaks with  $\text{KAu}(\text{CN})_2$  yielded a suitable derivative for which a 10-fold redundant data set was collected. A SIRAS phasing strategy produced a good quality 2.25 Å electron density map that was used for automated and manual building, interspersed with refinement, yielding a final model with an R-factor of 0.228 ( $R_{free} = 0.236$ ), with one TAB1 molecule in the asymmetric unit. TAB1 possesses an  $\alpha/\beta$  fold, formed by two stacked 5-stranded anti-parallel  $\beta$ -sheets, surrounded by  $\alpha$ -helices (Fig. 1B).

### The structure of TAB1 is similar to PP2C

Potential similarity between TAB1 and previously solved protein structures was investigated with a DALI search [13]. Strikingly, the structure most similar to TAB1 is that of PP2C $\alpha$  (PDB entry 1A6Q [14]), a metal-dependent protein serine/threonine phosphatase from the PPM family (Fig. 1B). The three-dimensional structure of PP2C $\alpha$  superimposes on TAB1 with an RMSD of 1.8 Å on 236 equivalent C $\alpha$  atoms (Fig. 1B). With the exception of the N-terminal  $\beta$ -strand, the entire

$\beta$ -sandwich of PP2C is conserved in TAB1. Similarly, the helices immediately surrounding the  $\beta$ -sandwich are topologically conserved between PP2C and TAB1. However, the three-helical bundle that makes up the C-terminal domain of PP2C is absent in the TAB1 structure, as a result of the TAB1 construct boundaries established by limited proteolysis. A structure-based sequence alignment reveals weak amino acid sequence homology between PP2C and TAB1 (17% identity, Fig. 2A). Notably, three large (10-29 residues) insertions are seen in the TAB1 structure/sequence compared to PP2C. Two of these (36-45 and 340-354) form a three-stranded anti-parallel  $\beta$ -sheet displayed on the TAB1 surface (Figs. 1,2). In addition, a single 29 residue insertion, consisting of two  $\alpha$ -helices, forms a stalk-like protrusion in TAB1 (Figs. 1,2). This stalk has a number of notable structural features. The two helices are amphipathic, with the hydrophobic faces interacting through small hydrophobic residues. Both basic and acidic side chains are displayed at the surface, six of which are involved in three salt bridges. The loop between the helices has an unusually high proline content (four out of fifteen residues, Fig. 2A) and is ordered in the electron density map. Structural similarity searches with the stalk fragment did not reveal similar protruding features on other known protein structures.

### **The active site of PP2C is partially conserved in TAB1**

Although TAB1 is topologically very similar to PP2C, the sequence conservation is low (Fig. 2A). When this sequence conservation is mapped onto the TAB1 surface (Fig. 2B), it becomes apparent that some of this sequence conservation locates to the area equivalent to the PP2C active site. PP2C possesses a highly negatively charged active site cleft, which is important for tight binding of the two catalytically important  $Mn^{2+}$  ions [14] (Fig. 2C). The TAB1 surface also appears to be

dominated by negative charges (Fig. 2C), although no ions were observed in the TAB1 structure. The extra  $\beta$ -sheet and stalk in TAB1 produce a much deeper groove than that observed for the active site in the PP2C structure.

Direct comparison of the PP2C active site with the equivalent region in TAB1 reveals a number of interesting similarities and differences. In PP2C, two  $Mn^{2+}$  ions are coordinated octahedrally through direct interactions with four aspartic acids, together with further coordination by protein-bound water molecules (Fig. 3A). In TAB1 grown in the absence of  $Mn^{2+}$ , no such ions are observed, and the equivalent space is taken up by four water molecules. Furthermore, only two of the six side chains directly or indirectly involved in metal coordination in PP2C are identical in TAB1 (Glu50 and Asp51, Figs. 2A, 3). The remaining four side chains have been substituted conservatively in TAB1 (Asn69, Glu290, Glu356 and Asp357). Interestingly, the roles of several of these PP2C metal binding residues have recently been investigated [15]. No significant effect on either turnover or substrate/metal binding was observed on mutation of Glu37 and Asp38, equivalent to the two residues conserved with TAB1. However, mutation of the PP2C Asp60 to Asn, identical to the substitution seen in TAB1 (Asn69), reduced  $k_{cat}$  by three orders of magnitude, together with a 40-fold increase in  $K_M$  for the metal. Similar deleterious effects on  $k_{cat}$  and  $K_M$  were seen for the PP2C D239N mutation. We found that the mutation of Asp239 to the residue found in TAB1 (Glu) abolished PP2C activity (Table II), suggesting that, although these substitutions in TAB1 are conservative, they greatly impair the ability of TAB1 to bind metals and perform catalysis.

The PP2C mutagenesis study also addressed the residues directly involved in catalysis [15]. PP2C is thought to hydrolyse the P-O bond through an acid/base catalytic mechanism, involving an activated water molecule [14, 15]. Asp282 (Glu356 in TAB1) is thought to be the catalytic base, ab-

strating a proton from a water molecule coordinated between the divalent metals. This water then performs nucleophilic attack on the phosphorus, leading to a pentavalent transition state. Protonation by a catalytic acid, thought to be His62 (Tyr71 in TAB1), is believed to produce a phosphate leaving group [15]. The negative charges of the substrate, transition state and product are thought to be stabilised through Arg33 (no equivalent in TAB1) and the mutation of this residue to Ala was found to decrease activity 20-fold [15]. Therefore, strikingly, none of these three catalytic residues are conserved in TAB1. We mutated Asp282 to the Glu found in TAB1 and this caused an approximately 10- to 40-fold reduction in the activity of PP2C towards either the synthetic phosphopeptide RRATpVA or *p*-nitrophenyl phosphate (Table II), similar to the 100-fold decrease observed by others towards *p*-nitrophenyl phosphate when Asp282 was mutated to Asn [15]. Previous studies had also shown a 20-fold decrease in  $k_{\text{cat}}$  towards *p*-nitrophenyl phosphate when His62 was changed to Gln and an 8-fold increase in the substrate  $K_{\text{M}}$  [15]. In agreement with this, we found that the mutation of His62 to the Tyr present in TAB1 results in an approximately 100-fold decrease in the activity of PP2C towards the peptide substrate (Table II). However, interestingly, towards the *p*-nitrophenyl phosphate, a two-fold increase in activity was observed. More detailed kinetic analysis indicated that the His62Tyr mutation increased the  $k_{\text{cat}}$  from  $0.076 \text{ min}^{-1}$  in the wild-type enzyme to  $0.152 \text{ min}^{-1}$  in the mutant, the  $K_{\text{M}}$  for *p*-nitrophenyl phosphate being unchanged at 10 mM. These observations suggest that His62 may not be the catalytic acid, but is involved in stabilising the leaving group required for the dephosphorylation of proteins and peptides, but not *p*-nitrophenyl phosphate. Furthermore, in a recently solved structure of a bacterial member of the PPM family, the equivalent residue is a methionine [16], suggesting that the identity of the catalytic acid in this family is as yet uncertain. In summary, these studies indicate that TAB1 is most unlikely to possess

catalytic activity similar to PP2C.

The structural and mutagenesis studies described above, suggest that TAB1 is not a catalytically active member of the PPM family of protein phosphatases. We therefore assayed TAB1 for protein phosphatase activity using either *p*-nitrophenyl phosphate or the peptide Arg-Arg-Ala-pThr-Val-Ala, which are two substrates employed commonly to measure PP2C [17]. No activity was detected towards either substrate in the presence of either 2 mM MnCl<sub>2</sub> or 10 mM MgCl<sub>2</sub>, even after prolonged incubation at 0.1 mg/ml TAB1. Although PP2C was originally described as an Mg<sup>2+</sup>-dependent enzyme, we also carried out experiments in the presence of Mn<sup>2+</sup>, because some protein phosphatases that are inactive in the presence of Mg<sup>2+</sup> do display activity in the presence of Mn<sup>2+</sup>.

#### **TAB1 binds a single manganese ion**

The crystal structure of PP2C $\alpha$  was solved using bacterially expressed enzyme grown and purified in the presence of Mn<sup>2+</sup> ions [14] and the published structure shows the presence of two manganese ions, despite the low metal affinity of PPM family members, with  $K_M$  values in the mM range [15]. Although no metal ions were observed in the TAB1 structure that we determined, this result was not definitive, because TAB1 was expressed in *E. coli* and purified in the absence of divalent cations. We therefore took three approaches to test the metal binding ability of TAB1. First, TAB1 was purified in the presence of millimolar concentrations of MnCl<sub>2</sub> and crystallised under similar conditions. This appeared to consistently produce poorly diffracting crystals (e.g. diffraction around 4 Å resolution). Second, native TAB1 crystals were soaked in millimolar concentrations of MnCl<sub>2</sub>. While this also affected diffraction unfavourably, a 3.5 Å data set was collected. An *F<sub>o</sub>-F<sub>c</sub>* differ-

ence electron density map was calculated using phases calculated from the refined TAB1 model. Strikingly, a  $13\sigma$  peak, presumably corresponding to a bound  $\text{Mn}^{2+}$  ion, was found in the active site (Fig. 3A). This peak corresponds approximately to the position of the second  $\text{Mn}^{2+}$  ion in the PP2C structure, interacting with three of the protein ligands (the Gly70 backbone and the Glu50/Asp51 side chains) that are conserved between TAB1 and PP2C (Figs. 2,3A).

Thirdly, to further investigate the affinity of the TAB1 active site for  $\text{Mn}^{2+}$  ions, isothermal titration microcalorimetry measurements were carried out (Fig. 3B). As expected for a highly charged ligand, the binding energy is dominated by a large negative enthalpic term ( $\Delta H = (-19 \pm 2)$  kJ mol<sup>-1</sup>), even though entropy gains ( $\Delta S = (35 \pm 7)$  J mol<sup>-1</sup> K<sup>-1</sup>) make a significant contribution to the free energy of binding ( $\Delta G = (-29.2 \pm 0.4)$  kJ mol<sup>-1</sup> and  $k_d = 8 \pm 2 \mu\text{M}$ ). With  $n = 0.84 \pm 0.06$  the fitted number of binding sites per TAB1 molecule is close to 1.0, the value expected from the crystal structure. These data support the notion that TAB1 binds a single  $\text{Mn}^{2+}$  ion in its active site with low micromolar affinity, in agreement with the crystallographic data.

## Concluding remarks

The evidence presented in this paper indicates that, despite its overall structural similarity to PP2C, TAB1 is unlikely to be catalytically active as a protein phosphatase. Key residues required for the binding of divalent cations and catalysis are lacking and TAB1 has no detectable activity towards two substrates normally used to assay protein phosphatases of the PPM family. Nonetheless, calorimetric and structural data suggest that TAB1 binds a single divalent cation with a significantly higher affinity compared to the PP2C active site. These observations raise the question of the physiological roles of the pseudophosphatase domain of TAB1.

Yeast adenylate cyclase possesses a PP2C-like domain that, like TAB1, lacks several residues involved in PP2C catalytic activity [14]. Strikingly, mutation of one of the remaining putative metal coordinating residues (equivalent to Asp38 in PP2C and Asp51 in TAB1) causes a 50-fold reduction in the activation of adenylate cyclase by Ras-GTP. It has been hypothesised that while the yeast adenylate cyclase does not possess PP2C-like phosphatase activity, the architecture of the active site could have been retained to provide a docking site for the  $\gamma$ -phosphate of GTP bound to Ras [14].

To the best of our knowledge, TAB1 is the first pseudophosphatase to be reported for the PPM family of protein phosphatases. For the protein tyrosine phosphatase family (PTP), several such inactive catalytic domains, known as STYX (phosphoSerine, phosphoThreonine or phosphoTyrosine interACTion proteins), have been reported [18]. These domains appear to have evolved from active PTPs, by mutation of the catalytic cysteine to a glycine, leading to proteins without phosphatase activity but with the retained ability to bind to phosphorylated proteins. The STYX proteins appear to act as anti-phosphatase proteins, preventing specific phosphorylated residues from becoming

dephosphorylated [18].

It has been reported that PP2C $\beta$ 1 interacts with TAK1 and is involved in the dephosphorylation and inactivation of the TAK1 catalytic subunit [19]. It is therefore possible that the interaction of the C-terminus of TAB1 with TAK1 not only induces TAK1 catalytic activity, but also positions the pseudophosphatase domain of TAB1 in such a way as to interact with TAK1 in a similar manner to PP2C $\beta$ 1, sterically preventing PP2C $\beta$ 1 from dephosphorylating and inactivating TAK1. We further speculate that the p38 $\alpha$  MAPK-catalysed phosphorylation of TAB1 induces a conformational change that facilitates the PP2C $\beta$ 1-catalysed inactivation of TAK1, which could underlie, at least in part, the feedback control of TAK1 activity by p38 $\alpha$  MAPK [5].

## Experimental Procedures

### **Tryptic digestion of full length human TAB1.**

Full length TAB1 was amplified from pET21a TAB1 [5] with a GC Rich PCR System (Roche) using oligonucleotides GCGGATCCGCGGCGCAGAGGAGGAGCT and GCGCGGCCCGCCTACGGT-GCTGTCACCACGCTC. The product was sub-cloned into pFBHTb (Invitrogen) to produce pFBHTb TAB1, which was expressed in insect Sf21 cells to produce full length His6-tagged TAB1. After purification on nickel nitrilotriacetate agarose and dialysis against 25 mM Tris/HCl pH 7.5, 150 mM NaCl, 0.1% (v/v) 2-mercaptoethanol, an aliquot (0.03 ml of a 0.8 mg/ml solution) was incubated for 30 min at 30 °C with 0-5 µg trypsin. The trypsinised fragments were denatured in SDS containing 5 mM benzamidine and subjected to SDS-PAGE and staining with Coomassie Colloidal Blue. The major 43 kDa protein staining fragment was subjected to Edman degradation to determine the N-terminal sequence, which showed that the fragment commenced at residue 7 of TAB1. The size of the fragment was estimated by calibrating the gel with marker proteins of known molecular mass, which indicated that the tryptic fragment was likely to terminate at Lys402.

### **Cloning, expression and purification of TAB1 [7-402]**

DNA encoding human TAB1[7-402] was amplified using oligonucleotides (GCGGATCCAGCTTGCT-GCAGAGTGAGCAGCAG) and (GCGGATCCTTACTTGCTGGTGCTCTGGGCGC). The resulting fragment was ligated into pCR2.1 (Invitrogen), sequenced then digested with *Bam*H1 and subcloned into the same site in pGEX6P-1 to form pGEX6P-1 TAB1[7-402], which expresses a glutathione-S-transferase-TAB1[7-402] fusion protein with a PreScission protease cleavage site between the GST and TAB1.

The human GST-TAB1[7-402] was expressed using *E. coli* BL21 (DE3) cells. The cells were grown at 37 °C to an A<sub>600</sub> of 0.6 in 5 l Luria-Bertani broth medium containing 100 µg/ml ampicillin, and then induced with 250 µM isopropyl-β-D-thiogalactopyranoside and grown for 16 h at 26 °C. The cells were harvested by centrifugation for 20 min at 3500 x g and then lysed by resuspension in 200 ml lysis buffer (50 mM Tris pH 7.5, 150 mM NaCl, 1 mM benzamidine, 1 mM phenylmethanesulphonyl fluoride and 0.1% (v/v) 2-mercaptoethanol), containing DNase I (0.1 mg/ml) and lysozyme (1 mg/ml). After incubation on ice for 30 min and brief sonication, the lysate was cleared by centrifugation for 30 min at 29,000 x g and incubated for 1 h at 4 °C with 7.5 ml of packed glutathione Sepharose beads (Amersham Biosciences). The resin was washed with 200 ml lysis buffer, 2 l 50 mM Tris/HCl pH 7.5, 500 mM NaCl, 0.1% (v/v) 2-mercaptoethanol and 500 ml 50 mM Tris/HCl pH 7.5, 300 mM NaCl, 0.1% (v/v) 2-mercaptoethanol and then resuspended in 15 ml of 50 mM Tris/HCl pH 7.5, 300 mM NaCl, 0.1% (v/v) 2-mercaptoethanol. Cleavage of the GST-TAB1[7-402] fusion was then performed by incubation with 200 µg GST-tagged PreScission protease for 16 h at 4 °C. The resulting supernatant was diluted in 50 mM Tris/HCl pH 7.5, 0.1% (v/v) 2-mercaptoethanol, in order to decrease the NaCl to 50 mM. The protein was loaded onto a Mono-Q HP column (Amersham Biosciences, Little Chalfont, UK) equilibrated in 50 mM Tris/HCl pH 7.5, 50 mM NaCl at a flow rate of 5 ml/min. The column was washed in the same buffer and the TAB1 was eluted with a linear 120 ml salt gradient from 0-0.5 M NaCl in the same buffer. Fractions of 1.5 ml were collected. The TAB1, which was eluted from Mono Q at 175 mM NaCl, was concentrated to 10 ml and loaded onto a 26/60 Superdex 200 gel filtration column equilibrated in 50 mM Tris/HCl pH 7.5, 300 mM NaCl, 1 mM dithiothreitol and the column developed on an AKTA Explorer system (Amersham Biosciences). The TAB1, which coincided with the

single peak of  $A_{280}$  absorbance was pooled, concentrated to 10 mg/ml and used for crystallisation.

### **Crystallisation, data collection, structure solution and refinement**

TAB1, was concentrated to 14.1 mg/ml, and crystallised by vapour diffusion. 1  $\mu$ l of protein was mixed with 1  $\mu$ l of mother liquor (100 mM HEPES pH 7.5, 1.5 M  $\text{Li}_2\text{SO}_4$ ) and 0.25  $\mu$ l 100 mM  $\text{BaCl}_2$ . Hexagonally-shaped crystals appeared within three days. Crystals were frozen in a nitrogen cryostream prior to data collection, using 100 mM HEPES pH 7.5, 1.5 M  $\text{Li}_2\text{SO}_4$  and 25% (v/v) glycerol. Soaks with metals  $\text{KAu}(\text{CN})_2$  and  $\text{MnCl}_2$ ) were performed by addition of 0.25  $\mu$ l of a 4-10 mM stock directly to the drop with the crystals. 4 mM  $\text{MnCl}_2$  was also part of the cryoprotecting solution used on the  $\text{MnCl}_2$ -soaked crystal. Synchrotron and rotating anode diffraction data were collected as shown in Table I.

Experimental phases were obtained from a SIRAS experiment, with the gold derivative and a low resolution (but more isomorphous) native data set, using HKL2MAP [20]. Two gold sites were located, and initial phases were calculated to 3.0 Å resolution. Solvent flattening and phase extension with the 2.25 Å native data set was then performed with DM [21], using a solvent content of 73%, assuming one molecule per asymmetric unit. This yielded a readily interpretable electron density map, from which warpNtrace [22] was able to automatically build 320 residues. Further refinement (with CNS [23]) and model building (with O [24] and COOT [25]) then yielded the final model with the statistics shown in Table I. Figures were made with PyMOL [26].

### **Isothermal titration microcalorimetry**

Thermodynamic data for  $Mn^{2+}$  binding to TAB1[7-402] were determined by isothermal titration microcalorimetry (ITC) using a VP-ITC instrument (Microcal, Inc.). All experiments were carried out at 25 °C with a protein concentration of 0.181 mM and a concentration of the ligand ( $MnCl_2$ ) of between 1.5 mM and 2.0 mM, both in 20 mM Tris/HCl pH 7.5 and 100 mM NaCl. The binding curve was measured in triplicate and a full set of background corrections was obtained. Data integration, correction and analysis were carried out using Origin 5 (Microcal, Inc.) with a single-set of sites binding model.

### **Cloning, expression, purification and assay of wild type and mutant PP2C $\alpha$ .**

DNA encoding PP2C $\alpha$  was amplified from pCW PP2C [14] using the GC Rich PCR System with oligonucleotides GCGGATCCATGGGAGCATTTTTAGACAAGCCAAAGATGG and GCGCGGC-CGCTTACCACATATCATCTGTTGATGTAGAGTCAGTG. The product was ligated into pCR2,1 (Invitrogen), sequenced and then sub-cloned into the *Bam*H1/*Not*I sites of pGEX6P-1. His62Tyr, Asp239Glu and Asp282Glu single mutants were then made using the Stratagene QuickChange Site-Directed Mutagenesis protocol. The wild type and mutant GST-PP2C fusions were expressed in *E. coli* (induced with 0.25 mM IPTG for 16 h at 26 °C), purified on glutathione Sepharose and dialysed against 50 mM Tris/HCl pH 7.5, 0.1 mM EGTA, 0.1% (v/v) 2-mercaptoethanol and aliquots stored frozen at -20 °C at 1-5 mg/ml.

The PP2C preparations were assayed at 26 °C in 50 mM Tris/HCl pH 7.5, 0.1 mM EGTA, 0.1% (v/v) 2-mercaptoethanol at concentrations ranging from 0.01-0.1 mg/ml using 5 mM *p*-nitrophenyl phosphate (5 mM) as substrate in the presence of 2 mM  $MnCl_2$  or 10 mM  $MgCl_2$ . The reactions (0.2

ml) were initiated with enzyme and initial velocities determined by monitoring the formation of *p*-nitrophenol from absorbance changes at 405 nm using a VersaMax microplate. PP2C preparations were also assayed at 26 °C using 1 mM of the synthetic phosphopeptide Arg-Arg-Ala-pThr-Val-Ala (where pThr is phosphothreonine) in the presence of either 2 mM MnCl<sub>2</sub> or 10 mM MgCl<sub>2</sub> [17]. The assays (0.025 ml) were stopped by the addition of 0.1 ml malachite green in 1 M HCl and, after incubation for 15 min, the phosphate released from the substrate was measured from the absorbance at 620 nm. Control experiments were carried out in which the PP2C was replaced by the buffer against which it was dialysed.

## Acknowledgements

We thank the European Synchrotron Radiation Facility, Grenoble, for the time at beamlines BM14 and ID14-3. DvA is supported by a Wellcome Trust Senior Research Fellowship and PC by a Royal Society Research Professorship. We thank Helge Dorfmueller, Vincent Rao and Fabrizio Villa for their help with crystallisation and data collection. We also thank different services within Division of Signal Transduction Therapy, School of Life Sciences, University of Dundee for the production of many of the reagents used in this study, the DNA Sequencing Service (coordinated by Nick Helps) for sequencing the constructs and the Protein Production and Assay development team (coordinated by Hillary Mclaughlan and James Hastie), for expression and purification of TAB1 and PP2C. We acknowledge the Medical Research Council, AstraZeneca, Boehringer-Ingelheim, GlaxoSmithKline, Merck and Co, Merck KGaA and Pfizer for financial support. The coordinates and structure factors have been deposited with the PDB (entry AAA, deposition in progress).

## Table I

Details of data collection & structure refinement. Values between brackets are for the highest resolution shell. All measured data were included in structure refinement.

	TAB1.high	TAB1.low	TAB1+KAu(CN) <sub>2</sub>	TAB1+MnCl <sub>2</sub>
Space group	P321	P321	P321	P321
Unit cell (Å)	a=b=141.97 c=65.91	a=b=143.41 c=66.04	a=b=143.42 c=66.25	a=b=141.26 c=65.75
Wavelength (Å)	1.03962	1.5418	1.03918	0.931
Resolution range (Å)	20–2.25 (2.33–2.25)	20–3.00 (3.11–3.00)	20–3.20 (3.31–3.20)	20–3.50 (3.62–3.50)
# Observed reflections	151048 (9864)	97559 (9627)	135233 (12182)	74851 (7828)
# Unique reflections	35816 (3001)	15778 (1535)	12874 (1243)	9779 (963)
Redundancy	4.2 (3.3)	6.2 (6.3)	10.5 (9.8)	7.7 (8.1)
I/σI	13.6 (2.3)	12.9 (3.9)	9.5 (5.1)	12.1 (6.0)
Completeness (%)	98.0 (82.4)	99.7 (99.7)	99.6 (98.0)	100.0 (100.0)
R <sub>merge</sub>	0.067 (0.467)	0.093 (0.542)	0.119 (0.466)	0.067 (0.428)
# Protein residues	355			
# Water molecules	83			
R, R <sub>free</sub>	0.228, 0.236			
RMSD from ideal geometry				
bonds (Å)	0.11			
angles (°)	1.8			
B-factor RMSD (Å <sup>2</sup> )				
(backbone bonds)	2.6			
<B> (Å <sup>2</sup> )				
protein	60.6			
water	52.7			

## Table II

Activities of wild type (WT) PP2C $\alpha$  and TAB1 and mutant forms of PP2C $\alpha$  towards two different substrates in the presence of magnesium or manganese ions. Activities towards the substrate RRATpVA (where Tp is phosphothreonine) are given as a percentage of that obtained with wild-type PP2C $\alpha$  in the presence of 10 mM Mg<sup>2+</sup>, while activities towards the substrate *p*-nitrophenyl phosphate (*p*NPP) are given as a percentage of that obtained with wild-type PP2C $\alpha$  in the presence of 2 mM Mn<sup>2+</sup>. The results are given  $\pm$  standard deviation for at least three determinations for each phosphatase preparation. BLD, below the level of detection.

Form of PP2C or TAB1	Substrate - RRATpVA		Substrate - <i>p</i> NPP	
	10 mM Mg <sup>2+</sup>	2 mM Mn <sup>2+</sup>	10 mM Mg <sup>2+</sup>	2 mM Mn <sup>2+</sup>
WT PP2C $\alpha$	100 $\pm$ 4	34.4 $\pm$ 0.4	18.3 $\pm$ 2.9	100 $\pm$ 6
PP2C $\alpha$ [H62Y]	0.69 $\pm$ 0.3	1.2 $\pm$ 0.1	54.5 $\pm$ 0.3	202 $\pm$ 14
PP2C $\alpha$ [D282E]	0.07 $\pm$ 0.01	0.9 $\pm$ 0.9	1.20 $\pm$ 10.01	1.1 $\pm$ 0.1
PP2C $\alpha$ [D239E]	BLD	BLD	<0.01	BLD
WT TAB1	BLD	BLD	<0.01	BLD

## Figure legends

### 1. The TAK1 signalling pathway and comparison of the TAB1 and PP2C folds.

A. TAK1 is activated in response to lipopolysaccharide (LPS) or pro-inflammatory cytokines (PIC), such as interleukin-1 (IL-1) and tumour necrosis factor (TNF). TAK1 then activates I $\kappa$ B kinase  $\beta$  (IKK $\beta$ ) leading to activation of the transcription factor NF $\kappa$ B and the COT protein kinase (also called tumour progression locus 2, Tpl2). COT then activates MKK1 and hence the extracellular signal-regulated kinases ERK1 and ERK2. TAK1 also activates other MKKs and hence their downstream substrates, the p38 $\alpha$  mitogen-activated protein kinase (MAPK) and c-Jun N-terminal kinases (JNK1/JNK2). The substrates for p38 $\alpha$  MAPK include the protein kinase MAPK-activated protein kinase 2 (MAPKAP-K2), while substrates for JNK include the transcription factors c-Jun and activating transcription factor 2 (ATF2). ERK1/ERK2 and MAPKAP-K2 trigger the production of PIC, such as tumour necrosis factor TNF, IL-6 and IL-8 by stabilising the mRNAs, stimulating the translation and/or the secretion of these PIC. The substrates for ERK1/ERK2 and MAPKAP-K2 that mediate these effects have not yet been fully defined. TAK1 is also subject to feedback regulation by p38 $\alpha$  MAPK, providing a mechanism for limiting the activation of several pro-inflammatory pathways in a coordinated manner [5].

B. The crystal structures of TAB1 and PP2C $\alpha$  (PDB entry 1A6Q [14]) are shown in a ribbon presentation. Helices are coloured red and strands are coloured blue, with the exception of TAB1 secondary structure elements that are not present in the PP2C structure (magenta helices, green strands). For the PP2C structure, the two active site Mn<sup>2+</sup> ions are shown as

magenta spheres, together with the observed reaction product, phosphate (sticks).

## 2. Structure-based sequence alignment of TAB1 and PP2C.

A. Structure-based sequence alignment of TAB1 and PP2C produced with ALINE (C.S. Bond, personal communication). TAB1 secondary structure elements are shown, using the same colour scheme as in Fig. 1B. PP2C residues that form direct or water-mediated interactions with the manganese ions are indicated by blue triangles. Further residues thought to participate in catalysis/substrate binding are indicated by yellow triangles.

B. Sequence conservation between TAB1 and PP2C, mapped onto a surface representation of the TAB1 structure. Grey = not conserved, green = conserved, dark green = similar residues.

C. Comparison of electrostatic surface potential (calculated with APBS [27]) of TAB1 and PP2C $\alpha$ , in the same orientation as Fig. 1B. Red is negatively charged (-5 kT), blue is positively charged (+ 5 kT). For PP2C $\alpha$ , the manganese ions and the phosphate are also shown.

## 3. Comparison of the TAB1 and PP2C active sites, metal binding to TAB1.

A. Stereo views of the active site structure of PP2C and the structurally equivalent region of TAB1. The protein backbones are shown as grey ribbons. Side chains are shown as sticks, those involved in metal binding or acid/base catalysis (green carbons) are labelled and also indicated in Fig. 2A. For PP2C, the manganese ions and associated water molecules are shown, together with the phosphate product. For TAB1, water molecules occupying approximately equivalent positions to the water molecules/metals in the PP2C structure are shown, together with the 3.5 Å  $F_o-F_c$  map ( $6\sigma$ ) resulting from the manganese soak (Table I). B. Isothermal titration microcalorimetry data for the binding of Mn<sup>2+</sup> to TAB1. The differential power signal from a representative experiment is shown on the left, the integrated

data (dots) and fitted curve (solid line) for the same experiment are shown on the right.

## References

- [1] Ninomiya-Tsuji, J., Kishimoto, K., Hiyama, A., Inoue, J., Cao, Z. D., and Matsumoto, K. (1999). The kinase TAK1 can activate the NIK-I $\kappa$ B as well as the MAP kinase cascade in the IL-1 signalling pathway. *Nature* **398**, 252–256
- [2] Lee, J., Mira-Arbibe, L., and Ulevitch, R. J. (2000). TAK1 regulates multiple protein kinase cascades activated by bacterial lipopolysaccharide. *J. Leukoc. Biol.* **68**, 909–915
- [3] Cheung, P. C. F., Nebreda, A. R., and Cohen, P. (2004). TAB3, a new binding partner of the protein kinase TAK1. *Biochem. J.* **378**, 27–34
- [4] Wang, C., Deng, L., Hong, M., Akkaraju, G. R., Inoue, J., and Chen, Z. J. J. (2001). TAK1 is a ubiquitin-dependent kinase of MKK and IKK. *Nature* **412**, 346–351
- [5] Cheung, P. C. F., Campbell, D. G., Nebreda, A. R., and Cohen, P. (2003). Feedback control of the protein kinase TAK1 by SAPK2a/p38 $\alpha$ . *EMBO J.* **22**, 5793–5805
- [6] Lee, J. C., Laydon, J. T., McDonnell, P. C., Gallagher, T. F., Kumar, S., Green, D., McNulty, D., Blumenthal, M. J., Heys, J. R., Landvatter, S. W., Strickler, J. E., McLaughlin, M. M., Siemens, I. R., Fisher, S. M., Livi, G. P., White, J. R., Adams, J. L., and Young, P. R. (1994). A protein-kinase involved in the regulation of inflammatory cytokine biosynthesis. *Nature* **372**, 739–746
- [7] Ge, B., Xiong, X., Jing, Q., Mosley, J. L., Filose, A., Bian, D., Huang, S., and Han, J. (2003). TAB1 $\beta$  (transforming growth factor- $\beta$ -activated protein kinase 1-binding protein 1 $\beta$ )

- ), a novel splicing variant of TAB1 that interacts with p38alpha but not TAK1. *J.Biol.Chem.* **278**, 2286–2293
- [8] Ge, B., Gram, H., Di Padova, F., Huang, B., New, L., Ulevitch, R. J., Luo, Y., and Han, J. (2002). MAPKK-independent activation of p38alpha mediated by TAB1-dependent autophosphorylation of p38alpha. *Science* **295**, 1291–1294
- [9] Kishimoto, K., Matsumoto, K., and Ninomiya-Tsuji, J. (2000). TAK1 mitogen-activated protein kinase kinase kinase is activated by autophosphorylation within its activation loop. *J.Biol.Chem.* **275**, 7359–7364
- [10] Ono, K., Ohtomo, T., Sato, S., Sugamata, Y., Suzuki, M., Hisamoto, N., Ninomiya-Tsuji, J., Tsuchiya, M., and Matsumoto, K. (2001). An evolutionarily conserved motif in the TAB1 C-terminal region is necessary for interaction with and activation of TAK1 MAPKKK. *J.Biol.Chem.* **276**, 24396–24400
- [11] Sakurai, H., Miyoshi, H., Mizukami, J., and Sugita, T. (2000). Phosphorylation-dependent activation of TAK1 mitogen-activated protein kinase kinase kinase by TAB1. *FEBS Lett.* **474**, 141–145
- [12] Brown, K., Vial, S. C. M., Dedi, N., Long, J. M., Dunster, N. J., and Cheetham, G. M. T. (2005). Structural basis for the interaction of TAK1 kinase with its activating protein TAB1. *J. Mol. Biol.* **354**, 1013–1020
- [13] Holm, L. and Sander, C. (1993). Protein structure comparison by alignment of distance matrices. *J.Mol.Biol.* **233**, 123–138

- [14] Das, A. K., Helps, N. R., Cohen, P. T. W., and Barford, D. (1996). Crystal structure of the protein serine/threonine phosphatase 2C at 2.0 Angstrom resolution. *EMBO J.* **15**, 6798–6809
- [15] Jackson, M. D., Fjeld, C. C., and Denu, J. M. (2003). Probing the function of conserved residues in the serine/threonine phosphatase PP2C $\alpha$ . *Biochemistry* **42**, 8513–8521
- [16] Pullen, K. E., Ng, H.-L., Sung, P.-Y., Good, M. C., Smith, S. M., and Alber, T. (2004). An alternate conformation and a third metal in PstP/Ppp, the *M. tuberculosis* PP2C-Family Ser/Thr protein phosphatase. *Structure* **12**, 1947–1954
- [17] Donella Deana, A., Mac Gowan, C. H., Cohen, P., Marchiori, F., Meyer, H. E., and Pinna, L. A. (1990). An investigation of the substrate specificity of protein phosphatase 2C using synthetic peptide substrates; comparison with protein phosphatase 2A. *Biochim.Biophys.Acta* **1051**, 199–202
- [18] Wishart, M. J. and Dixon, J. E. (1998). Gathering STYX: phosphatase-like form predicts functions for unique protein-interaction domains. *TIBS* **23**, 301–306
- [19] Hanada, M., Ninomiya-Tsuji, J., Komaki, K., Ohnishi, M., Katsura, K., Kanamaru, R., Matsumoto, K., and Tamura, S. (2001). Regulation of the TAK1 signaling pathway by protein phosphatase 2C. *J.Biol.Chem.* **276**, 5753–5759
- [20] Pape, T. and Schneider, T. R. (2004). Hkl2map: a graphical user interface for macromolecular phasing with shelx programs. *J.Appl.Cryst.* **37**, 843–844
- [21] Cowtan, K. (1994). dm: an automated procedure for phase improvement by density modification. *Joint CCP4 and ESF-EACBM Newsletter on Protein Crystallography* **31**, 34–38

- [22] Perrakis, A., Morris, R., and Lamzin, V. S. (1999). Automated protein model building combined with iterative structure refinement. *Nature Struct.Biol.* **6**, 458–463
- [23] Brunger, A. T., Adams, P. D., Clore, G. M., Gros, P., Grosse-Kunstleve, R. W., Jiang, J.-S., Kuszewski, J., Nilges, M., Pannu, N. S., Read, R. J., Rice, L. M., Simonson, T., and Warren, G. L. (1998). Crystallography and NMR system: A new software system for macromolecular structure determination. *Acta Crystallogr.* **D54**, 905–921
- [24] Jones, T. A., Zou, J. Y., Cowan, S. W., and Kjeldgaard, M. (1991). Improved methods for building protein models in electron density maps and the location of errors in these models. *Acta Crystallogr.* **A47**, 110–119
- [25] Emsley, P. and Cowtan, K. (2004). Coot: model-building tools for molecular graphics. *Acta Crystallogr.* **D60**, 2126–2132
- [26] DeLano, W. L. (2004). Use of pymol as a communications tool for molecular science. *Abstr.Pap.Am.Chem.Soc.* **228**, 030–CHED
- [27] Baker, N. A., Sept, D., Joseph, S., Holst, M. J., and McCammon, J. A. (2001). Electrostatics of nanosystems: application to microtubules and the ribosome. *Proc. Natl. Acad. Sci. USA* **98**, 10037–10041

# Figure 1

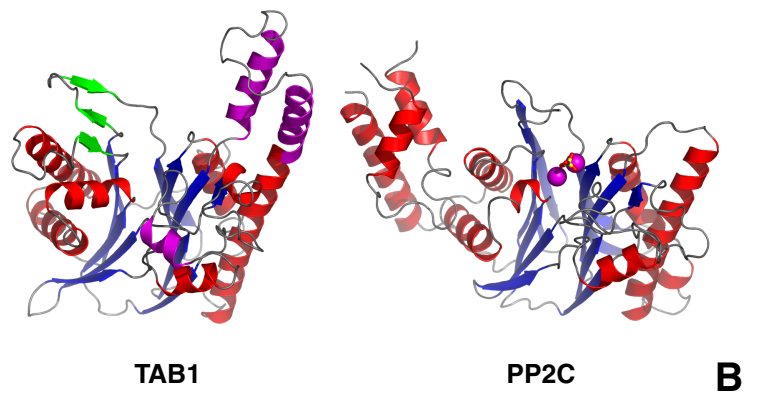
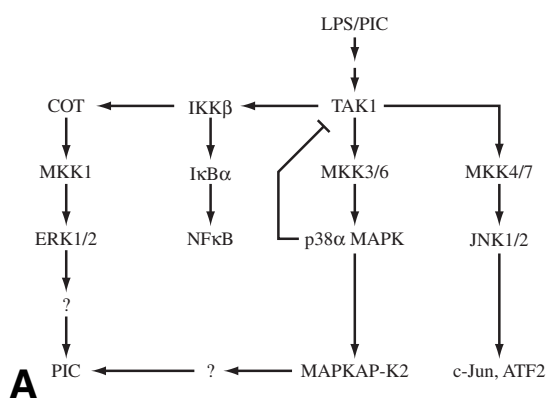




Figure 3

